A TIME-STAGGERED SECOND ORDER SCHEME FOR MOIST AIR VARIABLE DENSITY FLOW

Hector Amino, Cédric Flageul, Bertrand Carissimo, Martin Ferrand, Jean-Marc Hérard

The 8th European Congress on Computational Methods in Applied Sciences and Engineering
ECCOMAS Congress 2022
5–9 June 2022, Oslo, Norway

A TIME-STAGGERED SECOND ORDER SCHEME FOR MOIST AIR VARIABLE DENSITY FLOW

H. Amino[1,2], C. Flageul[3], B. Carissimo[1,2], M. Ferrand[1,2], J.M. Hérard[1,2]

[1]EDF R&D, Fluid Mechanics, Energy and Environment Dept., Chatou, France
martin.ferrand@edf.fr

[2] CEREA, Ecole des Ponts, EDF R&D, Chatou, France

[3] PPRIME Institute, Curiosity Group, Université de Poitiers, CNRS, ISAE-ENSMA, France

Key words: Finite volumes, compressible flow, incompressible flow, pressure correction, phase change, homogeneous model

1 Introduction

When simulating moist air flow with phase change, one may differentiate the homogeneous models and the two fluid approach. The first considers the fluid as an unique pseudo compound, a mixture, composed of both air and water components [1][2][3]; therefore, the flow can be treated as if it has one phase, leading to a more simplified set of equations. The second solves equations for both gas and liquid phases, which can be computationally more expensive but is more accurate when the phasic disequilibrium is important [4]. In the homogeneous models framework, if the fluid components are ideal gases, the mixture thermodynamic expressions can be written as combinations of analytic formulas.

Moreover, simulating variable density flow at all speed is an active topic of research, with many application in the industrial field. Different classes of scheme exist going from the incompressible to the compressible range. In this context, several semi-implicit all-speed schemes, designed to avoid stability constraints related to the acoustic waves and based on the asymptotic preserving method have been proposed in the last decades (see [5] for instance).

Additionally, recent work addressed a strategy of using high-order schemes to capture unsteady flow phenomena. Based on pioneer works for incompressible flow [6], Pierce and Moin [7] proposed a time staggered second order finite differences scheme for variable-density flow using the low Mach assumption. The latter was extended in [10] to the finite volumes method and compressible Navier–Stokes equations, by solving an Helmholtz equation for the pressure, which removes any time step constraint related to the acoustic waves, and also by conserving the total energy thanks to the resolution of the internal energy equation with a corrective source term, based on [8].

In this paper, we extend the pressure correction [9] time staggered scheme from [10] to moist air applications, while keeping the numerical properties presented in [10]. The homogeneous model is considered and the phase change between the liquid and vapor water phase is accounted for using a Newton method on the solved internal energy. This is possible by assuming a volume fraction of the liquid phase small compared to the gaseous ones. After presenting the chosen governing equations, section 2 introduces

the main steps of the discrete time scheme. Then, an analysis on the thermodynamical quantities is performed and a verification is carried out on two analytical test cases.

2 Governing equations

A mixture of air and water in liquid and vapor phases is considered with respectively the indexes (a), (l) and (v). The mixture total water mass fraction is denoted y_w, with $y_w = y_v + y_l$. Its motion, studied with the continuum hypothesis in a bounded space Ω, is described by the Navier–Stokes compressible equations:

$$\begin{aligned}
&(a)\ \ \frac{\partial \rho}{\partial t} + \mathrm{div}\left(\underline{q}\right) = 0,\\
&(b)\ \ \frac{\partial \underline{q}}{\partial t} + \underline{\mathrm{div}}\left(\underline{u}\otimes\underline{q}\right) = -\underline{\nabla} p + \underline{\mathrm{div}}\left(\underline{\underline{\tau}}\right) + \underline{f},\\
&(c)\ \ \frac{\partial (\rho\, e)}{\partial t} + \mathrm{div}\left(e\underline{q}\right) = -p\,\mathrm{div}\left(\underline{u}\right) + \underline{\underline{\tau}} : \underline{\underline{\nabla u}} + \mathrm{div}\left(\lambda \underline{\nabla} T\right),\\
&(d)\ \ \frac{\partial (\rho\, y_w)}{\partial t} + \mathrm{div}\left(y_w \underline{q}\right) = \mathrm{div}\left(K \underline{\nabla} y_w\right),\\
&(e)\ \ p = p_a + p_v = \rho\, R_a\, T\left[y_a + y_v \varepsilon_m^{-1}\right].
\end{aligned} \tag{1}$$

ρ is the density of the mixture, $\underline{q} = \rho \underline{u}$ its momentum and e its internal energy. Note that $y_a + y_w = 1$. Since the water liquid volume fraction α_w is negligible towards the water vapor volume fraction α_v, the mixture pressure p is the sum of the partial pressures of dry air and water vapor following the Dalton law [14]. ε_m is the ratio between the molar masses of water and air. $\underline{f}$ is the field of volume force (*e.g.* gravity force $\rho \underline{g}$), $\underline{\underline{\tau}} = \mu\left(\underline{\underline{\nabla u}} + \underline{\underline{\nabla u}}^T\right) + \left(\kappa - \frac{2}{3}\mu\right)\mathrm{div}\left(\underline{u}\right)\underline{\underline{I}}$, is the shear stress tensor. κ is the volume viscosity, which is usually neglected and is omitted in this article. $R_a = R/M_a$ is the specific dry air constant. Additional source terms are not considered here.
The mixture temperature is directly linked to the internal energy through

$$e = c_{v_m} T + y_v L_0, \tag{2}$$

where c_{v_m} is the mixture heat capacity defined as $c_{v_m} = y_a c_{v_a} + y_v c_{v_v} + y_l c_{v_l}$, with the different components capacities considered constant. In case of saturation, the water vapor mass fraction y_v is calculated using the absolute humidity at saturation X_s:

$$y_v = \frac{X_s}{1 + X_s}, \qquad \text{where} \quad X_s = \frac{\varepsilon_m p_s}{p - p_s}.$$

$p_s = \exp\left(A + \dfrac{B.t}{C + t}\right)$ is the pressure at saturation calculated using the Antoine's law, with t the temperature in Celsius. Combining the last definitions, the expression of the water vapor mass fraction y_v in saturation can be written as a function of the temperature and pressure:

$$y_v(T, p) = \frac{\varepsilon_m p_s(T)}{p - (1 - \varepsilon_m) p_s(T)}. \tag{3}$$

3 Discrete notations

To ease the discrete spatial and time integration of the equations, in the next section the important discrete notations are presented below. The mean space values overs a cell c and its face f are:

$$(.)_c := \frac{1}{\Omega_c}\int_c (.)\mathrm{d}\Omega, \qquad (.)_f := \frac{1}{S_f}\int_f (.)\mathrm{d}S. \tag{4}$$

Ω_c and S_f are the cell volume and surface respectively. The mean time value over the time interval $[t^n, t^{n+1}]$ is denoted by:

$$(.)|_n^{n+1} := \frac{1}{\Delta t}\int_{t^n}^{t^{n+1}} (.)\mathrm{d}t, \tag{5}$$

where Δt is the interval measure. Moreover, the time values at time t^n and t^{n+1} are written with the superscript $(.)^n$ and $(.)^{n+1}$, respectively. The time interval $\Delta t|_n^{n+1}$ is then $t^{n+1} - t^n$.

In the present numerical scheme, the time stepping is defined by the parameter θ, bounded in $[0,1]$. We consider the cases where $\theta = 1$ (implicit Euler, 1^{st} order time interpolation of $(.)|_n^{n+1}$) and $\theta = 1/2$ (Crank Nicolson, 2^{nd} order time interpolation of $(.)|_n^{n+1}$). A field ψ time interpolation $\Theta\left(\psi^n, \psi^{n+1}\right)$ between times n and $n+1$ is defined as:

$$\Theta\left(\psi^n, \psi^{n+1}\right) := (1-\theta)\,\psi^n + \theta\psi^{n+1}.$$

The dual time interval around time n is denoted by $[n-1+\theta, n+\theta]$, and is of length:

$$\Delta t|_{n-1+\theta}^{n+\theta} := \Theta\left(\Delta t|_{n-1}^{n},\, \Delta t|_n^{n+1}\right),$$

From the above expressions, the extensive quantities such as the cell mass M_c, velocity $\underline{u}_c$, momentum $\underline{Q}_c$ and face mass flux $\dot{M}_f$ are defined as follows:

$$M_c := \int_c \rho\mathrm{d}\Omega, \qquad \underline{u}_c = \frac{\underline{Q}_c}{M_c}, \qquad \underline{Q}_c := \int_c \rho\underline{u}\mathrm{d}\Omega, \qquad \dot{M}_f := \int_f \underline{q}\cdot\underline{dS} = \underline{q}_f\cdot\underline{S}_f.$$

Finally, discrete spatial operators (denoted by capital letters) are defined. The discrete operator divergence of a face-averaged field $\underline{\Psi}_f$ is as follows:

$$\mathrm{Div}_c\left(\underline{\Psi}_f\right) := \frac{1}{\Omega_c}\sum_{f\in\mathcal{F}_c}\underline{\Psi}_f\cdot\underline{S}_f = \left(\mathrm{div}\left(\underline{\Psi}\right)\right)_c, \tag{6}$$

where $\mathcal{F}_c$ is the ensemble of all the planar polygonal faces of the cell c, and $\underline{S}_f$ is the outward surface vector. The discrete cell gradient operator of a field ψ is also defined as the divergence of the tensor $\psi\underline{\underline{I}}$:

$$\underline{\mathrm{Grad}}_c\left(\psi_f\right) := \frac{1}{\Omega_c}\sum_{f\in\mathcal{F}_c}\psi_f\underline{S}_f = \left(\underline{\mathrm{div}}\left(\psi\underline{\underline{I}}\right)\right)_c. \tag{7}$$

Finally, the discrete Laplacian operator of a given scalar ψ with coefficient of diffusion K uses the two points flux approximation (TPFA) (see [15] and [16] for more details) and is defined as:

$$\mathrm{Lapl}_c\left(K,\,\psi\right) := \frac{1}{\Omega_c}\sum_{f\in\mathcal{F}_c}K\underline{\nabla}_f\psi\cdot\underline{S}_f, \qquad \underline{\nabla}_f\psi = \frac{\psi_{\widetilde{c}} - \psi_c}{d_{c\widetilde{c}}}. \tag{8}$$

4 Numerical scheme

The time staggered theta-scheme published in [10] is extended to an ideal gas mixture here. An iterative process is proposed with inner-iterations denoted by the superscript k, starting at 1. The approach combines a prediction and correction steps, which is classically used in incompressible schemes. Two pressure are distinguished. The mixture thermodynamic pressure, located with the other thermodynamic variables (denoted as p^n for the time t^n) can be differentiated from the mechanical pressure which applies a force on the momentum during the time interval $[n-1+\theta, n+\theta]$ (denoted by $p|_{n-1+\theta}^{n+\theta}$):

$$p^{n+1,k} = \frac{1}{\theta} p|_{n-1+\theta}^{n+\theta,k} + \frac{\theta-1}{\theta} p|_{n-2+\theta}^{n-1} + p_0 \tag{9}$$

For simplicity, a constant time step Δt is supposed in this section.

Time integration

for $n \in [0, N-1]$

- *Initialisation:* for $k=0$, the cell c initial values are

$$\rho_c^{n,0} = \rho_c^{n-1}, \quad \rho_c^{n+1,0} = \rho_c^n, \quad \underline{q}_f\Big|_n^{n+1,0} \cdot = \underline{q}_f\Big|_{n-1}^{n}, \quad p_c|_{n-1+\theta}^{n+\theta,0} = p_c|_{n-2+\theta}^{n-1+\theta}.$$

  As a side note, at any iteration, the mass flux should verify the following mass balance equation:

$$\mathrm{Div}_c\left(\underline{q}_f\Big|_n^{n+1,k}\right) = -\frac{\left(\rho_c^{n+1,k} - \rho_c^{n,k}\right)}{\Delta t}.$$

Sub-iterations for $k \in [0, M-1]$

- *Buoyant scalars step:* The water mass fraction $y_w^{n+1,k}$ and the internal energy $e^{n+1,k}$ are computed by solving in the interval $[n, n+1]$:

$$\begin{aligned}
&(\mathrm{a}): \ \frac{\rho_c^{n+1,k-1} y_{wc}^{n+1,k} - \rho_c^{n,k-1} y_{wc}^{n}}{\Delta t} + \mathrm{Div}_c\left(\left\langle \Theta\left(y_w^n, y_w^{n+1,k}\right)\right\rangle_f \underline{q}_f\Big|_n^{n+1,k-1}\right) = \mathrm{Lapl}_c\left(K, \Theta\left(y_w^n, y_w^{n+1,k}\right)\right), \\
&(\mathrm{b}): \ \frac{\rho_c^{n+1,k-1} e_c^{n+1,k} - \rho_c^{n,k-1} e_c^{n}}{\Delta t} + \mathrm{Div}_c\left(\left\langle \Theta\left(e^n, e^{n+1,k}\right)\right\rangle_f \underline{q}_f\Big|_n^{n+1,k-1}\right) = \mu(S_c^2)^{n+\theta,k-1} + \Gamma_c^{u^2/2}\Big|_n^{n+1,k-1} \\
&+ \mathrm{Lapl}_c\left(\lambda, \Theta\left(T^n, T^{n+1,k}\right)\right) - \mathrm{Div}_c\left(\left\langle \Theta\left(p^n, p^{n+1,k-1}\right)\underline{u}^{n+\theta,k-1}\right\rangle_f\right) + \underline{u}_c^{n+\theta,k-1} \cdot \underline{\nabla}_c p|_{n-1+\theta}^{n+\theta,k-1}.
\end{aligned} \tag{10}$$

  The term $(p\mathrm{div}(\underline{u}))_c$ is implemented as $\mathrm{Div}_c(p\underline{u}) - \underline{u}_c \cdot \underline{\nabla}_c(p)$. Different spatial discretisations can be used for the convective terms (see [17] for more details). For the first sub-iteration, $\rho^{n,k-1}$ is ρ^{n-1} and $\rho^{n+1,k-1}$ is ρ^n; thus, the density variation $(\rho^n - \rho^{n-1})$ is balanced by the mass flux $\underline{q}_f\Big|_{n-1}^{n} \cdot \underline{S}_f$ term. $\Gamma_c^{u^2/2}\Big|_n^{n+1,k-1}$ is a corrective source term derived from the discrete kinetic energy

equation based on [8] and is derived here for the present sub-iterative scheme:

$$\Gamma_c^{u^2/2}\Big|_n^{n+1,k-1} = \frac{\Theta\left(\rho_c^n, \rho_c^{n+1,k-2}\right)}{\Theta\left(\rho_c^n, \rho_c^{n+1,k-1}\right)}\Theta\left(\rho_c^{n-1}, \rho_c^n\right)\frac{\left[|\underline{u}_c^{k-1} - \underline{u}_c^{n-1+\theta}|^2\right]}{2\Delta t}$$
$$+\left[1 - \frac{\Theta\left(\rho_c^n, \rho_c^{n+1,k-2}\right)}{\Theta\left(\rho_c^n, \rho_c^{n+1,k-1}\right)}\right]\left[\Theta\left(\rho_c^{n-1}, \rho_c^n\right)\frac{|\underline{u}_c^{n-1+\theta}|^2}{2\Delta t} - \mathrm{Div}_c\left(\frac{\left|\left\langle\Theta\left(\underline{u}^{n-1+\theta}, \widetilde{\underline{u}}^{k-1}\right)\right\rangle_f\right|^2}{2}\underline{q}_f\Big|_{n-1+\theta}^{n+\theta,k-2}\right)\right]$$
$$-\frac{\Theta\left(\rho_c^n, \rho_c^{n+1,k-2}\right)}{\Theta\left(\rho_c^n, \rho_c^{n+1,k-1}\right)}\mathrm{Div}_c\left(\frac{\left|\left\langle\Theta\left(\underline{u}^{n-1+\theta}, \widetilde{\underline{u}}^{k-1}\right)\right\rangle_f - \underline{u}_c^{k-1}\right|^2}{2}\underline{q}_f\Big|_{n-1+\theta}^{n+\theta,k-2}\right). \tag{11}$$

This term is important in order to be consistent related to singular solution by conserving the total energy. More details concerning its derivation is given in [10].

- The mixture temperature $T^{n+1,k}$ is computed from the mixture internal energy using Equation (2). Considering a constant pressure $p^{n+1,k-1}$ and total water mass fraction $y_{wc}^{n+1,k}$, the internal energy expression can be written as:

$$e_c^{n+1,k} = \left[(1 - y_{wc}^{n+1,k})c_{va} + y_{vc}^{n+1,k}c_{vv} + (y_{wc}^{n+1,k} - y_{vc}^{n+1,k})c_{vl}\right]T_c^{n+1,k} + y_{vc}^{n+1,k}L_0. \tag{12}$$

The water vapor mass fraction is the water mass fraction if the cell volume is not saturated. Otherwise,

$$y_v^{n+1,k} = \frac{\varepsilon_m p_{sat}(T^{n+1,k})}{p^{n+1,k-1} - (1-\varepsilon_m)\,p_{sat}(T^{n+1,k})}, \quad p_{sat}(T^{n+1,k}) = \exp\left(A + \frac{B(T^{n+1,k} - T_0)}{C + T^{n+1,k} - T_0}\right). \tag{13}$$

T_0 is the reference temperature fixed here as 273.15 K. Equation (12) is then written following $T^{n+1,k}$. The Newton method is used to compute the temperature $T^{n+1,k}$ in case of saturation. Thus, an iterative process inside the inner iteration, denoted by the superscript l, is performed to compute the temperature respecting the Equation (12) at a given precision, fixed by the user:

$$T_c^{n+1,k,l} = \frac{e_c^{n+1,k} - e_c^{n+1,k,l-1}}{\left.\dfrac{\partial e}{\partial T}\right|_{p,y_w}\left(p_c^{n+1,k-1}, y_{wc}^{n+1,k}, T_c^{n+1,k,l-1}\right)} + T_c^{n+1,k,l-1}. \tag{14}$$

The initial temperature $T_c^{n+1,k,0}$ and internal energy $e_c^{n,n+1,0}$ depend on the previous cell volume state (i.e saturated or not). $y_{vc}^{n+1,k}$ and $y_{lc}^{n+1,k}$ are then updated with the new temperature value.

- An intermediate density is calculated with the equation of state

$$\widetilde{\rho}_c^k = \frac{p_c^{n+1,k-1}}{R_a T_c^{n+1,k-1}\left[1 - y_{wc}^{n+1,k} + y_{vc}^{n+1,k}\varepsilon_m^{-1}\right]}$$

This new density is not balanced by any mass flux. The mass conservation is insured in the correction step.

- *Prediction step*: An intermediate velocity $\widetilde{\underline{u}}^k$ is computed by solving the momentum equation in the time interval $[n-1+\theta, n+\theta]$:

$$\frac{\Theta\left(\rho_c^n, \rho_c^{n+1,k-1}\right)\widetilde{\underline{u}}_c^k - \Theta\left(\rho_c^{n-1}, \rho_c^{n,k-1}\right)\underline{u}_c^{n-1+\theta}}{\Delta t} + \mathrm{Div}_c\left(\left\langle \Theta\left(\underline{u}^{n-1+\theta}, \widetilde{\underline{u}}^k\right)\right\rangle_f \otimes \underline{q}_f\Big|_{n-1+\theta}^{n+\theta,k-1}\right)$$
$$= -\underline{\mathrm{Grad}}_c\left(\left\langle p\big|_{n-1+\theta}^{n+\theta,k-1}\right\rangle_f\right) + \underline{\mathrm{Div}}_c\left(\underline{\underline{\tau}}_f^k\right) + \underline{f}_c\Big|_{n-1+\theta}^{n+\theta,k-1}. \tag{15}$$

$\underline{q}_f\Big|_{n-1+\theta\ \ f}^{n+\theta,k-1}$ is defined by $\underline{q}_f\Big|_{n-1+\theta}^{n+\theta,k-1} = \Theta\left(\underline{q}_f\Big|_{n-1}^{n}, \underline{q}_f\Big|_{n}^{n+1,k-1}\right)$. Note that the cell pressure gradient and external volume force are taken at the same time interval; if they are in a partial balance, no parasite velocities are created.

- *Correction step:* During this stage, the pressure increment $\phi^k = p\big|_{n-1+\theta}^{n+\theta,k} - p\big|_{n-1+\theta}^{n+\theta,k-1}$ is computed and used to correct the density, pressure and velocity. The mass equation and a simplified momentum equation are combined leading to a Helmholtz equation solved on $[n, n+1]$:

$$\frac{\rho_c^{n+1,k} - \rho_c^n}{\Delta t} - \theta\mathrm{Lapl}_c\left(\Delta t, p^{n+1,k}\right) = -\mathrm{Div}_c\left(\left\langle \Theta\left(\rho^n, \rho^{n+1,k-1}\right)\widetilde{\underline{u}}^k + \Delta t\left(\underline{\nabla} p\big|_{n-1+\theta}^{n+\theta,k-1} + \delta\underline{f}^k\right)\right\rangle_f\right)$$
$$+ (1-\theta)\mathrm{Lapl}_c\left(\Delta t, p\big|_{n-2+\theta}^{n-1+\theta}\right). \tag{16}$$

Note that the Rhie and Chow filter [11] is used in Equation (16) and the density $\rho^{n+1,k}$ reads:

$$\rho_c^{n+1,k} = \widetilde{\rho_c}^{\,k} + \left(p_c^{n+1,k} - p_c^{n+1,k-1}\right)\left(\left.\frac{\partial\rho}{\partial p}\right|_T\left(T_c^{n+1,k}, p_c^{n+1,k-1}\right)\right). \tag{17}$$

The thermodynamic pressure $p^{n+1,k}$ is linked to ϕ^k through:

$$\phi_c^k = \Theta\left(p_c\big|_{n-2+\theta}^{n-1+\theta}, p_c^{n+1,k}\right) - p_c\big|_{n-1+\theta}^{n+\theta,k-1}. \tag{18}$$

Finally, the velocity $\underline{u}^{n+\theta,k}$ is corrected:

$$\underline{q}_f\Big|_n^{n+1,k} = \left\langle \Theta\left(\rho^n, \rho^{n+1,k}\right)\underline{u}^{n+\theta,k}\right\rangle_f = \left\langle \Theta\left(\rho^n, \rho^{n+1,k-1}\right)\widetilde{\underline{u}}^k\right\rangle_f - \Delta t\left(\underline{\nabla}_f\phi^k - \delta\underline{f}_c^k\right), \tag{19}$$

which verifies the mass balance with $\dfrac{\rho_c^{n+1,k} - \rho_c^n}{\Delta t}$, and whose field face values are calculated using a centred scheme.

The correction (17) makes the scheme conservative in space and time for mass, which is an important property for non-regular solutions. From a generic point of view, the density $\rho^{n+1,k}$ in equation (17) might not satisfy the equation of state (contrary to what was done in step 6 of [7]). The sub-iterative process for the time step ends when the error $\varepsilon^k = \sqrt{\sum_{c=1}^{N_{cell}} \Omega\left|\underline{u}^{n+\theta,k} - \underline{u}^{n+\theta,k-1}\right|^2}$ is below a fixed value ε_0.

5 Properties

New Courant and Fourier conditions are described in this section to insure the positivity of the internal energy, pressure and density. An upwind spatial discretisation of the convective terms is considered.

5.1 Internal energy

For $k > 1$ and using, Equation (10) for the internal energy is written:

$$\begin{aligned}
&\left[M_c^n \frac{e_c^{n+1,k} - e_c^n}{\Delta t|_n^{n+1}} + \sum_{f \in \mathcal{F}_c} \left(\left\langle \Theta\left(e^n, e_c^{n+1,k}\right) \right\rangle_f - e_c^{n+1,k} \right) \dot{M}_f|_n^{n+1,k-1} \right] \\
&+ \sum_{f \in \mathcal{F}_c} \lambda |\underline{S}_f| \frac{\Theta\left(T_c^n, T_c^{n+1,k-1}\right) - \Theta\left(T_{\widetilde{c}}^n, T_{\widetilde{c}}^{n+1,k-1}\right)}{d_{c\widetilde{c}}} = \Omega_c \mu (S_c^2)^{n+\theta} + \Gamma_c^{u^2/2}\Big|_n^{n+1,k-1} \\
&- \sum_{f \in \mathcal{F}_]} \left\langle \Theta\left(p^n, p^{n+1,k-1}\right) \underline{u}^{n+\theta,k-1} \right\rangle_f \cdot \underline{S}_f + \Omega_c \underline{u}_c^{n+\theta,k-1} \cdot \underline{\nabla}_c p|_{n-1+\theta}^{n+\theta,k-1}.
\end{aligned} \tag{20}$$

The equation (20) yields a linear system $\underline{\underline{A}}\underline{X} = \underline{B}$, where $\underline{X} = (e_c)_{c \in \{1,..,N_{cell}\}}$. Considering the cell initial internal energy, λ, R_a, and Δt positive, $\underline{\underline{A}}$ is diagonal dominant and a M-matrix if:

$$CFL_{T_1}^+ < 1, \qquad \text{where } CFL_{T_1}^+ = (1-\theta)\frac{\Delta t}{M_c^n} \sum_{f \in \mathcal{F}_c} \dot{M}_f^+\Big|_n^{n+1,k-1}. \tag{21}$$

$$\begin{aligned}
CFL_{T_2}^+ < 1, \quad \text{where } CFL_{T_2}^+ = \frac{\Delta t}{M_c^n} \sum_{f \in \mathcal{F}_c} &\left[(1-\theta) + \frac{R_a \Theta\left(T_c^n, T_c^{n+1,k-1}\right)}{e_c^n} \right] \dot{M}_f^+\Big|_n^{n+1,k-1} \\
&+ \frac{\Delta t \underline{u}_c^{n+\theta,k-1} \cdot \underline{\nabla}_c p|_{n-1+\theta}^{n+\theta,k-1}}{\rho_c^n e_c^n}..
\end{aligned} \tag{22}$$

$$Fo_T^+ < 1, \qquad \text{where } Fo_T^+ = \frac{\lambda_c \Delta t}{M_c^n} \sum_{f \in \mathcal{F}_c} \frac{\Theta\left(T_c^n - T_{\widetilde{c}}^n, T_c^{n+1,k-1} - T_{\widetilde{c}}^{n+1,k-1}\right)}{e_c^n d_{c\widetilde{c}}}. \tag{23}$$

5.2 Pressure equation

The Helmholtz equation to solve the pressure increment for $k > 1$ is written with the spatial discretisation:

$$\begin{aligned}
&\frac{\Omega_c p_c^{n+1,k}}{\Delta t} \frac{\partial \rho}{\partial p}\bigg|_T (p_c^{n+1,k-1}, T_c^{n+1,k}) - \theta \Delta t \sum_{f \in \mathcal{F}_c} \underline{\nabla}_f p_c^{n+1,k} \cdot \underline{S}_f = \frac{\rho_c^n \Omega_c}{\Delta t} + (1-\theta)\Delta t \sum_{f \in \mathcal{F}_c} \underline{\nabla}_f p|_{n-2+\theta}^{n-1+\theta} \cdot \underline{S}_f \\
&- \sum_{f \in \mathcal{F}_c} \left\langle \Theta\left(\rho^n, \rho^{n+1,k-1}\right) \widetilde{\underline{u}}^k + \Delta t \underline{\nabla}_c p|_{n-1+\theta}^{n+\theta,k-1} \right\rangle_f \cdot \underline{S}_f.
\end{aligned} \tag{24}$$

$$\frac{\partial \rho}{\partial p}\bigg|_T (p_c^{n+1,k-1}, T_c^{n+1,k}) = \frac{1}{R_a T_c^{n+1,k}\left[1 - y_{wc}^{n+1,k} + y_{v_c}^{n+1,k}\varepsilon_m\right]}, \qquad y_{v_c}^{n+1,k} = \frac{\varepsilon_m p_{sat}(T_c^{n+1,k})}{p_c^{n+1,k-1} - (1-\varepsilon_m)\, p_{sat}(T_c^{n+1,k})}$$

If the internal energy is positive so is the temperature and the vapor pressure at saturation p_{sat}. $\left.\frac{\partial \rho}{\partial p}\right|_T (p_c^{n+1,k-1}, T_c^{n+1,k})$ is strictly positive if ${y_{vc}}^{n+1,k}$ is, i.e.:

$$p_c^{n+1,k-1} > (1-\varepsilon_m)\, p_{sat}(T_c^{n+1,k}). \tag{25}$$

Equation (24) yields a linear system $\underline{\underline{A}}\,\underline{X} = \underline{B}$, where $\underline{X} = (p_c^{n+1,k})_{c\in\{1,..,N_{cell}\}}$. Considering the cell internal energy, λ, R_a, and Δt positive, $\underline{\underline{A}}$ is diagonal dominant and a M-matrix if the condition (25) and the following CFL condition are respected:

$$CFL_p^+ < 1, \quad \text{where } CFL_p^+ := \frac{\Delta t}{\rho_c^n \Omega_c^n} \sum_{f\in\mathcal{F}_c} a_f^\phi, \tag{26}$$

and

$$a_f^\phi = \left\langle \Theta\left(\rho^n, \rho^{n+1,k-1}\right) \widetilde{\underline{u}}^k + \Delta t \underline{\nabla} p|_{n-1+\theta}^{n+\theta,k-1} \right\rangle_f \cdot \underline{S}_f - (1-\theta)\Delta t \underline{\nabla}_f p|_{n-2+\theta}^{n-1+\theta} \cdot \underline{S}_f.$$

6 Verification

Three verification cases are chosen to test the moist air time scheme. We recall that the present work is based on a dry air second order time scheme for variable density flow [10] which was widely verified and validated on different incompressible and compressible test cases.

6.1 0-D closed cavity with phase change

A single $[1 \times 1 \times 1]$ m cell is first considered to evaluate the treatment of the water phase change by the presented scheme. During 10 s, an outgoing heat flux ($Q = 100\,\mathrm{W\,m^{-2}}$) is imposed on the lateral walls, then, the same flux is injected back from 10 s to 20 s. Other walls are considered adiabatic. The time step is $\Delta t = 1$ s and 1 inner iteration is performed. The initial temperature and pressure are $T_0 = 293.15\,\mathrm{K}$ and $p_0 = 101\,325\,\mathrm{Pa}$. The cell total water mass fraction is constant and equal to $y_w = 0.125$. With the system internal energy variation, the cell reaches saturation and the liquid and vapor water mass fractions change over time.

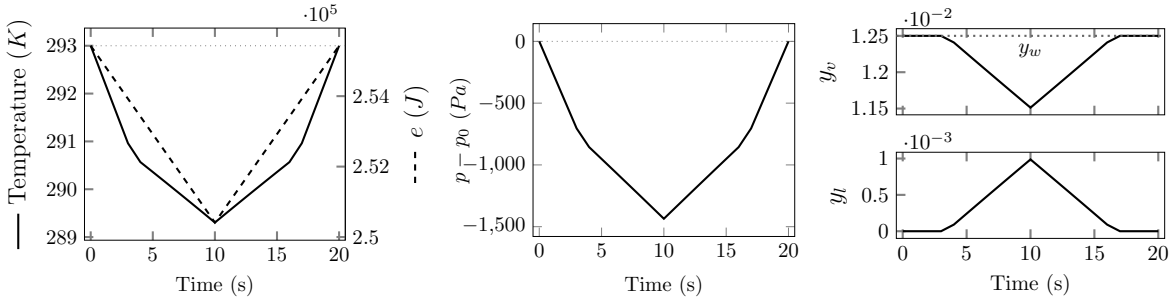

Figure 1: Variables evolution following time. Left: temperature and internal energy. Middle: pressure. Right: water mass fractions.

As shown in Figure 1, the initial state is recovered for all studied variables. It is observed as well that the saturation is reached, changing the slope of the temperature variation, but not the internal energy one.

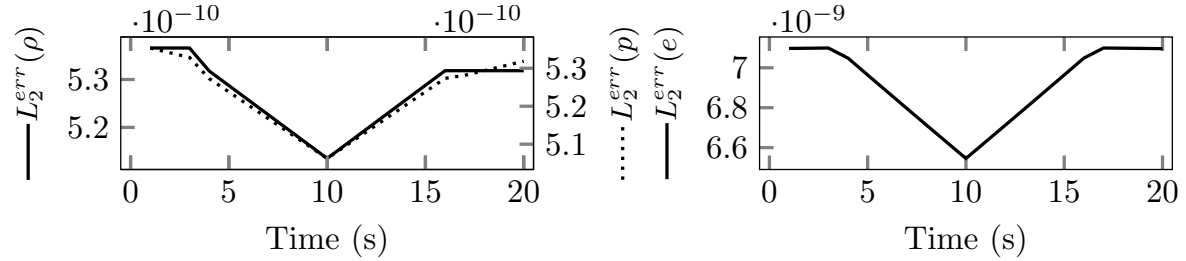

Figure 2: Variables L_2 error norm evolution following time. Left: density and pressure. Right: internal energy.

Note that the sum of the water vapor and liquid mass fraction is always equal to the total water mass fraction, which is in agreement with the chosen moist air model. Moreover, Figure 2 shows the density, internal energy and pressure (for the given temperature and water vapor mass fraction) L_2 normalised error norm. For the three variables, the error is below the solver precision of 10^{-8}, emphasising the simulation accuracy.

6.2 Riemann problem associated to the system

6.2.1 Proposition

- The one-dimensional Riemann problem associated with the System (1), disconsidering the diffusive terms, admits an unique self-similar solution $\underline{W}(\xi)$, with $\xi = x/t$, with no vacuum occurrence, if and only if the following condition (27) holds on the initial data:

$$\underline{W}(x<0,t=0) = \underline{W}_L, \quad \underline{W}(x>0,t=0) = \underline{W}_R,$$

which reads:

$$u_R - u_L < \frac{2}{\Gamma(y_{wR})-1} c_R + \frac{2}{\Gamma(y_{wL})-1} c_l, \tag{27}$$

with c and Γ defined as following:

$$c(y_w,\rho,p) = \left(\frac{p}{\rho}\Gamma(y_w)\right)^{\frac{1}{2}}, \qquad \Gamma(y_w) = \frac{R_a(1-y_w(1-\varepsilon^{-1}))}{c_{vm}} + 1. \tag{28}$$

- The solution is composed by constant intermediate states, $\underline{W}_L$, $\underline{W}_1$, $\underline{W}_2$ and $\underline{W}_R$, separated respectively by genuinely nonlinear 1-4 waves associated with the eigenvalues $\lambda_{1/4} = u \pm c$ and a contact discontinuity associated with the double system eigenvalue $\lambda_{2-3} = u$.

The proof is classically obtained by construction [18] using the Rankine–Hugoniot conditions and considering the entropy inequality:

$$\frac{\partial(\rho s)}{\partial t} + \mathrm{div}\,(\rho s \underline{u}) < 0, \tag{29}$$

where $s(y_w,\rho,p) = p\rho^{-\Gamma(y_w)}$.
Two test cases are studied to verify the scheme accuracy related to the presented Riemann problem. First, an Unsteady Contact Discontinuity (UCD) is considered followed by a Double Symmetric Shock (DSS)

problem. No phase change is considered and the simulations are carried out on grids with $2^m \times M_0$ cells, $0 \leq m \leq 5$, with $M_0 = 800$ for the UCD and 80 for the DSS. The initial conditions are given in Table 1. The computational domain is a tube of length $L = 400\,\mathrm{m}$ for the UCD and $L = 40\,\mathrm{m}$ for the DSS, extending from $x = -L/2$ to $x = L/2$, the interface being located at $x = 0\,\mathrm{m}$. Symmetry conditions are imposed on all boundary faces of the computational domain except at the two end faces of the tube, which are set to be outlets. For each case, the fields L_1 error norm (related to the Riemann problem exact solution ψ_e, Eq.(30)) is studied for $\theta = 1$, and a constant $CFL = 0.04$ at $t = 0.3\,\mathrm{s}$ for the UCD and $t = 0.03\,\mathrm{s}$ for the DSS.

Test	y_L	T_L[K]	u_L[m s^{-1}]	p_L[Pa]	y_R	T_R[K]	u_R[m s^{-1}]	p_R[Pa]
UCD	0.01	300	2.0	100,000	0.015	320	2.0	100,000
DSS	0.0125	293.0	10.0	100,000	0.0125	293.0	-10.0	100,000

Table 1: Initial states for the two one-dimensional Riemann problems used.

$$L_1^{err}(\psi) = \frac{\sum_{c=1}^{N_c} |\Omega_c| \; |\psi_e(x_c) - \psi_c|}{\sum_{c=1}^{N_c} |\Omega_c| \; |\psi_e(x_c)|}. \tag{30}$$

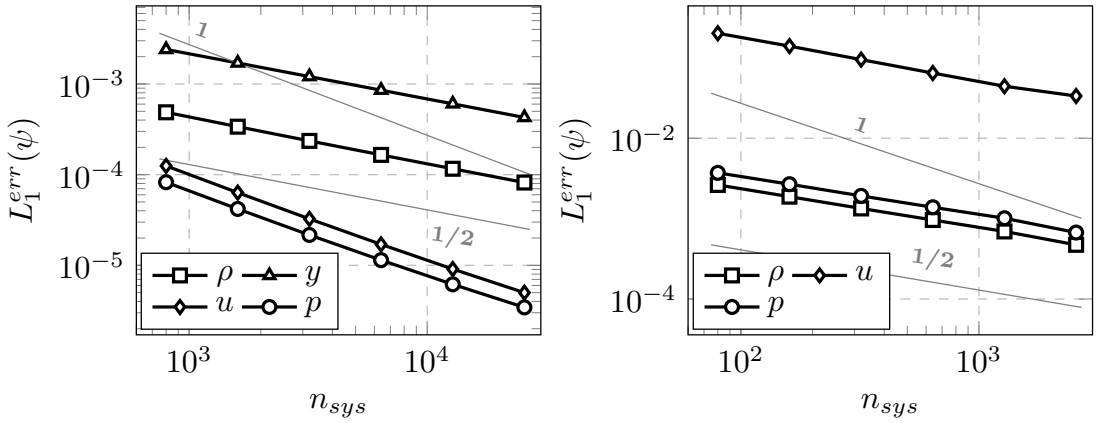

Figure 3: Variables L_1 error norm for (right) UCD at $t = 0.05\,\mathrm{s}$, (left) DSS at $t = 0.3\,\mathrm{s}$.

Figure 3 shows the L_1 error norm for the different system variables given the mesh refinement. It is observed that for both UCD and DSS cases, the numerical scheme is consistent compared to the exact solution. Moreover, for the UCD, the density and water mass fraction, have a convergence rate of $\frac{1}{2}$ whereas the pressure and velocity convergence rate is close to 1, which is expected [19]. For the DSS, all the variables present a convergence rate of $\frac{1}{2}$, which is expected as well [19](the error for the total

water mass fraction was exactly 0 for the DSS). Figures 4 and 5 show the good agreement between the numerical results and the problems exact solutions while the mesh is refined.

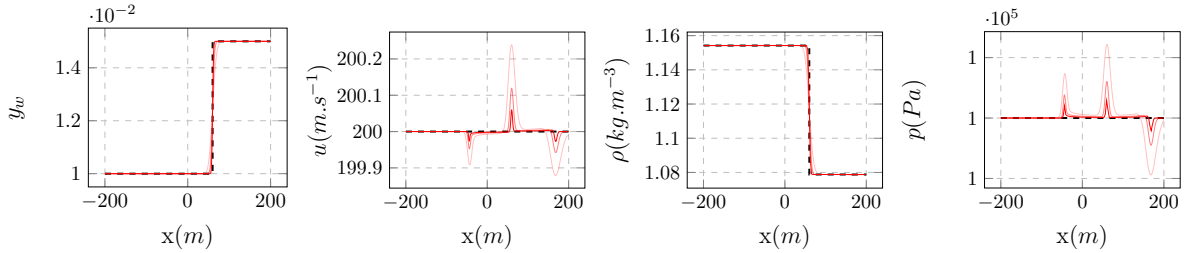

Figure 4: UCD case fields at $t = 0.3\,\mathrm{s}$ for different mesh refinements (800, 3200, 12800). (- -) Exact solution. (–) Simulation.

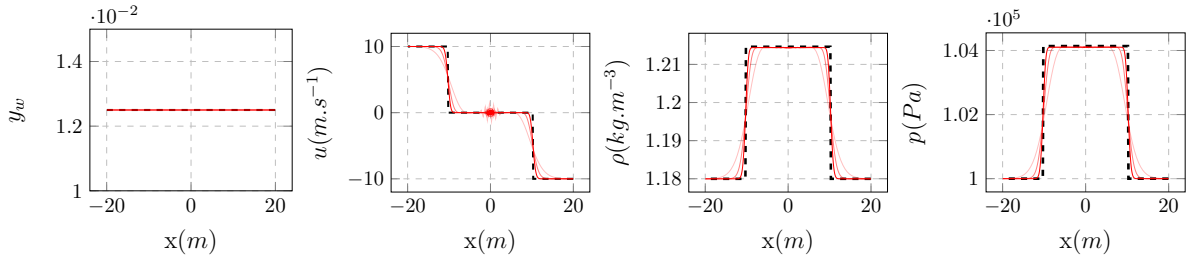

Figure 5: DSS case fields at $t = 0.03\,\mathrm{s}$ for different mesh refinements (80, 320, 1280). (- -) Exact solution. (–) Simulation.

7 CONCLUSIONS

A second order time scheme for most air variable density flow was implemented in the open source CFD solver code_saturne. The Navier–Stokes compressible equations are used; a Helmholtz equation is solved for the pressure correction, avoiding any time step constraint related to acoustic waves while taking into account the pressure variation. The total energy is conserved by solving the mixture internal energy equation completed with a corrective source term. The phase change is accounted for by a Newton method used to compute the temperature from the solved internal energy. The second order is achieved thanks to a time staggered variable arrangement. A numerical analysis is carried out on the positivity of the thermodynamic variables, leading to three new stability conditions,which shall be further studied in the future works.

The scheme was verified on two different problems. First, its ability to take into account the water phase change was tested on a 0-D volume. Then, two Riemann problems were studied, with no phase change considered, where the numerical results were shown to be consistent in relation to the exact solutions. Concerning the model application range, one should not forget the hypothesis of small volume fraction of liquid (i.e. on indoor environments for instance).

Further work shall focus on the presented scheme validation against references and experimental data with phase change, notably by taking into account the diffusive effects.

REFERENCES

[1] Clerc, S. (2000). Numerical simulation of the homogeneous equilibrium model for two-phase flows. Journal of Computational Physics, 161(1), 354-375.

[2] Hurisse, O. (2017). Numerical simulations of steady and unsteady two-phase flows using a homogeneous model. Computers Fluids, 152, 88-103.

[3] Downar-Zapolski, P., Bilicki, Z., Bolle, L., Franco, J. (1996). The non-equilibrium relaxation model for one-dimensional flashing liquid flow. International journal of multiphase flow, 22(3), 473-483.

[4] Hérard, J. M., Hurisse, O. (2012). A fractional step method to compute a class of compressible gas–liquid flows. Computers Fluids, 55, 57-69.

[5] Degond, P., Tang, M. (2011). All speed scheme for the low Mach number limit of the isentropic Euler equations. Communications in Computational Physics, 10(1), 1-31.

[6] Crank, J., Nicolson, P. (1947, January). A practical method for numerical evaluation of solutions of partial differential equations of the heat-conduction type. In Mathematical Proceedings of the Cambridge Philosophical Society (Vol. 43, No. 1, pp. 50-67). Cambridge University Press.

[7] Pierce, C. D., Moin, P. (2004). Progress-variable approach for large-eddy simulation of non-premixed turbulent combustion. Journal of fluid Mechanics, 504, 73-97.

[8] Herbin, R., Latché, J. C., Zaza, C. (2020). A cell-centred pressure-correction scheme for the compressible Euler equations. IMA Journal of Numerical Analysis, 40(3), 1792-1837.

[9] Guermond, J. L., Minev, P., Shen, J. (2006). An overview of projection methods for incompressible flows. Computer methods in applied mechanics and engineering, 195(44-47), 6011-6045.

[10] Amino, H., Flageul, C., Benhamadouche, S., Tiselj, I., Carissimo, B. and Ferrand, M. (2022), A time-staggered second order conservative time scheme for variable density flow. Int J Numer Meth Fluids. Accepted Author Manuscript. https://doi.org/10.1002/fld.5116

[11] Rhie, C. M., Chow, W. L. (1983). Numerical study of the turbulent flow past an airfoil with trailing edge separation. AIAA journal, 21(11), 1525-1532.

[12] Zienkiewicz, O.C. and Taylor, R.L. *The finite element method*. McGraw Hill, Vol. I., (1989), Vol. II., (1991).

[13] Idelsohn, S.R. and Oñate, E. Finite element and finite volumes. Two good friends. *Int. J. Num. Meth. Engng.* (1994) **37**:3323–3341.

[14] Dalton, J. (1802). Essay IV. On the expansion of elastic fluids by heat. Memoirs of the Literary and Philosophical Society of Manchester, 5(2), 595-602.

[15] Eymard, R., Gallouët, T., Guichard, C., Herbin, R., Masson, R. (2014). TP or not TP, that is the question. Computational Geosciences, 18(3), 285-296.

[16] Ferrand, M., Fontaine, J., Angelini, O. (2014). An Anisotropic Diffusion Finite Volume Algorithm Using a Small Stencil. In Finite Volumes for Complex Applications VII-Elliptic, Parabolic and Hyperbolic Problems (pp. 577-585). Springer, Cham.

[17] Archambeau, F., Méchitoua, N., Sakiz, M. (2004). Code Saturne: A finite volume code for the computation of turbulent incompressible flows-Industrial applications. International Journal on Finite Volumes, 1(1).

[18] Smoller, J. (2012). Shock waves and reaction—diffusion equations (Vol. 258). Springer Science Business Media.

[19] Gallouët, T., Hérard, J. M., Seguin, N. (2002). Some recent finite volume schemes to compute Euler equations using real gas EOS. International journal for numerical methods in fluids, 39(12), 1073-1138.